Biochimica et Biophysica Acta 1827 (2013) 1148–1155

Contents lists available at ScienceDirect

Biochimica et Biophysica Acta

journal homepage: www.elsevier.com/locate/bbabio

Molecular dynamics simulations reveal highly permeable oxygen exit channels shared with water uptake channels in photosystem II

Serguei Vassiliev *, Tatiana Zaraiskaya, Doug Bruce

Department of Biology, Brock University, 500 Glenridge Ave, St. Catharines L2S 3A1, Canada

ARTICLE INFO

Article history:
Received 19 April 2013
Received in revised form 14 June 2013
Accepted 18 June 2013
Available online 28 June 2013

Keywords:
Photosystem II
Oxygen permeation
Molecular dynamics

ABSTRACT

Photosystem II (PSII) catalyzes the oxidation of water in the conversion of light energy into chemical energy in photosynthesis. Water delivery and oxygen removal from the oxygen evolving complex (OEC), buried deep within PSII, are critical requirements to facilitate the reaction and minimize reactive oxygen damage. It has often been assumed that water and oxygen travel through separate channels within PSII, as demonstrated in cytochrome c oxidase. This study describes all-atom molecular dynamics simulations of PSII designed to investigate channels by fully characterizing the distribution and permeation of both water and oxygen. Interestingly, most channels found in PSII were permeable to both oxygen and water, however individual channels exhibited different energetic barriers for the two solutes. Several routes for oxygen diffusion within PSII with low energy permeation barriers were found, ensuring its fast removal from the OEC. In contrast, all routes for water showed significant energy barriers, corresponding to a much slower permeation rate for water through PSII. Two major factors were responsible for this selectivity: (1) hydrogen bonds between water and channel amino acids, and (2) steric restraints. Our results reveal the presence of a shared network of channels in PSII optimized to both facilitate the quick removal of oxygen and effectively restrict the water supply to the OEC to help stabilize and protect it from small water soluble inhibitors.

1. Introduction

Molecular oxygen participates in numerous cellular processes and interacts with a variety of reaction sites within many different proteins. Due to its small size and nonpolar nature oxygen has generally been accepted to exhibit relatively unconstrained movement through proteins to and from these active sites [6]. However, this point of view is changing as a number of studies (hydrogenase [9], myoglobin [8], aquaporin [40], copper amine oxidazes [21], flavoenzymes [3], cytochrome c oxidase [24], fluorescent proteins [7,27], lipoxygenases [29] and amino acid oxidases [28]) have revealed the presence of specific oxygen diffusion channels. Experimental localization of molecular oxygen within proteins remains challenging. O_2 is highly mobile and is usually not resolved in X-ray crystal structures. One successful strategy involves mimicking oxygen with xenon or krypton, which should have similar binding properties but higher electron densities. X-ray structures of proteins loaded with these inert gases have revealed potential oxygen binding sites [33]. Other techniques, like tryptophan fluorescence quenching [11] are more coarse grained in nature and suffer from relatively low spatial resolution. The use of computational methods to identify minimal energy locations for molecular oxygen within proteins could potentially serve as an alternative "molecular microscope" [10].

Photosystem II (PSII) is the enzyme that uses sunlight to oxidize water and reduce plastoquinone [2,14] in the process of oxygenic photosynthesis. Molecular oxygen is released at the active site of the water splitting complex of PSII and finds its way through the protein to the lumen and eventually to the atmosphere. PSII drives this reaction with an abundant extraterrestrial energy source, the sun, which ultimately powers most forms of life on our planet. The onset of oxygenic photosynthesis was transformative, causing mass extinctions of anaerobic life forms and enabling the dominance of a diverse group of aerobic life forms.

Structural and mechanistic details of water splitting and oxygen release are not well understood. PSII is a ~350 kDa complex of 20 protein subunits embedded in the thylakoid membranes of green plant chloroplasts, and internal membranes of cyanobacteria [35]. The heart of PSII's unique ability of direct solar water oxidation is the oxygen-evolving complex (OEC), a Mn_4CaO_5 cluster embedded in the reaction center D1 polypeptide and separated from the bulk lumenal water by extrinsic protein subunits. In cyanobacteria these extrinsic subunits are PsbO, PsbU and PsbV (Fig. 1).

Even before detailed knowledge of the structure of PSII was available, water channels had been suggested to be important for optimal binding and orientation of substrate water as well as for restricting the access of unwanted solutes and reactions associated with excessive amounts of water [1,42]. Oxygen channels were also thought to

Abbreviations: PSII, photosystem II; PMF, potential of mean force; ROS, reactive oxygen species; OEC, oxygen-evolving complex; ILS, implicit ligand sampling

* Corresponding author. Tel.: +1 905 6885550x6140; fax: +1 905 6881855.
E-mail address: svassiliev@brocku.ca (S. Vassiliev).

0005-2728/$ – see front matter © 2013 Elsevier B.V. All rights reserved.
http://dx.doi.org/10.1016/j.bbabio.2013.06.008

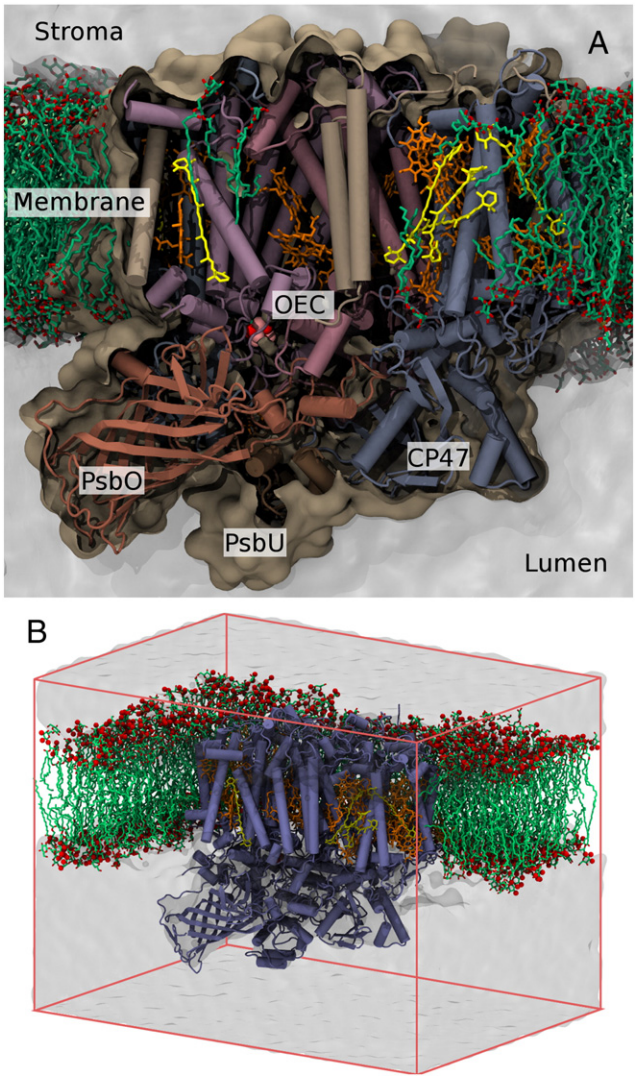

Fig. 1. (A) The structure of Photosystem II. The catalytic oxygen-evolving complex (OEC) is located roughly in the middle of the solvent exposed part of the protein and is shown using red (oxygen atoms) and pink (manganese atoms) spheres. The PsbO, PsbU and CP47 subunits shield OEC from the bulk water; the PsbV subunit is located behind CP47 in this diagram. (B) A setup of a molecular dynamics simulation. A simulation system is composed of *Thermosynechococcus vulcanus* PSII core complex (PDB ID: 3ARC) embedded in a lipid bilayer membrane and a water solvent box. Membrane is clipped for clarity.

be important for the fast removal of this reactive product from the protein, and especially photoactive pigments, to minimize oxidative damage and production of reactive oxygen species (ROS) [1].

Elucidation of the X-ray structure of PSII [12,23] confirmed that the Mn_4CaO_5 cluster is buried within PSII, and gave the first insights into details of substrate and product conduction. Several channels were identified in a number of computational studies examining internal solvent accessible surfaces found within the crystallographic structures of PSII [13,18,25]. Channels were tentatively assigned to carry water, oxygen or protons based solely on their width and the relative abundance of hydrophilic aminoacids lining them. A significant limitation of these initial studies was that only one static conformation of the protein complex was considered. However, the PSII protein as well as the channels within it, are dynamic at physiological temperatures [9,17]. To identify water channels from a dynamic point of view, molecular dynamics (MD) simulations of a PSII core complex were performed [37], and the energetic barriers for water permeation though PSII extrinsic polypeptides were determined [38]. These studies found a system of branching pathways of water diffusion in PSII connecting the OEC to a number of distinct entrance points on the lumenal surface. Gibbs free energy profiles for water permeation indicated that water access is restricted to some degree in all of the observed channels. The main constriction sites were identified and suggested to serve as selectivity filters restricting both the access of solutes detrimental to the water oxidation reaction and loss of Ca^{2+} and Cl^{-} from the active site [38]. Molecular dynamics studies supported the original idea that regulatory mechanisms exist to control substrate access to the Mn_4CaO_5 cluster [38] and revealed mechanistic details of this process.

In contrast to water, oxygen permeation in PSII has not been studied as extensively. As described above, early computational cavity searches of X-ray structures assigned the more hydrophobic static channels to oxygen. The only experimental result related to molecular oxygen diffusion within PSII was an X-ray structural study which revealed two krypton binding sites [13]. Recently we described a computational approach to discovery of pathways for molecular oxygen through molecular dynamics simulated structures [43]. We applied an implicit ligand sampling technique to generate a 3D map for the free energy of molecular oxygen within PSII that was then analyzed with a wavefront propagation algorithm to find the lowest energy pathways for oxygen. This approach revealed two potential oxygen channels leading from the OEC to the bulk water in the lumen that appeared to show significant overlap with previously described water channels.

Key questions regarding water and oxygen channels remain: are there unique channels for oxygen release in PSII? Do oxygen and water share channels? Does PSII preferentially employ a single pathway or a multitude of routes to optimize the release of oxygen? To address these questions we have employed a variety of computational techniques to investigate the topology of oxygen release channels and determine permeation barriers for both water and oxygen within PSII.

While water is relatively abundant in the interior of PSII, oxygen is not. Computational approaches previously used successfully to follow water movement in PSII, based on equilibrium molecular dynamics, diffusion tensor imaging [37] or accelerated water injection [38] were dependent on the relatively large numbers of water molecules and cannot be simplistically applied to identify oxygen pathways. We thus applied a two step approach to the discovery and characterization of oxygen channels within PSII based on our previous work with implicit ligand sampling (ILS). A comprehensive application of the ILS method was followed by the determination of accurate free energy profiles for both water and oxygen along new oxygen pathways and all previously found water channels using simulations with explicit water and oxygen ligands.

Our study establishes a detailed atomistic model for the release of oxygen from PSII and compares it to the uptake of water. Oxygen and water are shown to share channel systems which display differential permeability to the two solutes.

2. Methods

2.1. Set up of the system for molecular dynamics simulations

The simulation setup was similar to that described in [37] with modifications based on the most recent 1.9 Å resolution X-ray structure of the PSII core complex [35]. The simulation system (Fig. 1) included all protein subunits of the first PSII core complex monomer from PDB ID: 3ARC. The following modifications were applied. Crystal water was kept and additional water molecules were added using the DOWSER program [44]. The protocol used by the DOWSER program was to place water in internal cavities, relax them to minimize their interaction energy, and finally to select and retain only water molecules with interaction energies below −12 kcal/mol. The threshold water–protein interaction energy was set to this value which had

previously been found to be optimal for distinguishing hydrated cavities from empty cavities [44]. The MD simulations were done with NAMD 2.8 [22] and performed with periodic boundary conditions at constant pressure (1 atm) and temperature (300 K) using Langevin dynamics with Nosé-Hoover Langevin piston pressure control. The long range electrostatic interactions were calculated using the particle-mesh Ewald algorithm with grid spacing 1 Å. Both the electrostatic and the Lennard-Jones interactions were cutoff at 12 Å. Smoothing functions were applied at 10 Å. The AMBER ff99SB force field [39] with modification of the ϕ/ψ dihedral parameters as in [30] was used for protein and the GLYCAM-2000a force field [4] was used for the headgroups of galactolipids. The force field for cofactors was based on the parameters described previously [36]. Only nonbonding interactions between atoms in the OEC were included. OEC atoms and distances between OEC and its ligands were constrained with internal bond constraints with a force constant of 2 kcal/(mol·A^2). The protein alpha carbons were constrained to their X-ray crystallographic positions with a force constant of 2 kcal/(mol·A^2). The system was equilibrated for 2 ns before production runs. The entire system including the PSII complex, the membrane patch and TIP3P water contained approximately 320,000 atoms. MCCE 2.4 [31] was used to sample the ionization state of each protein residue. Protonation states were kept fixed in molecular dynamics simulations.

2.2. Implicit ligand sampling (ILS) calculations

A three dimensional free energy map was calculated for the presence of molecular oxygen within PSII using implicit ligand sampling as previously described [43]. In this approach the free energy associated with the placement of an implicit oxygen molecule at any point within the protein is calculated. Our free energy map for molecular oxygen was computed using a total of 10,000 snapshot structures taken from a 10 ns long MD simulation of PSII. The grid spacing was 0.5 Å and at each point the free energy of an oxygen molecule was determined for 12 different orientations of that molecule. Lennard-Jones parameters and the O–O bond length for oxygen molecules were taken from [16]: $\sigma = 1.507$ Å, $\varepsilon = -0.097$ kcal/mol, O–O bond length = 1.22 Å. The ILS calculations were performed with version 1.9 of the VMD program [20].

2.3. The search for channels within a 3D free energy map

To determine potentially favorable oxygen pathways through PSII we propagated a wave front through the three dimensional free energy map using the Eikonal equation:

$$|\nabla t(\mathbf{x})| = s(\mathbf{x})$$

where $s(\mathbf{x})$ is the "slowness" of the medium and $t(\mathbf{x})$ represents the arrival time of a wave front at point $\mathbf{x}$. This method is described in detail in [43]. The Eikonal equation was solved using the finite differences method as implemented in the FDTIMES package [26]. The result of this calculation is a three dimensional map of the first arrival time computed for all points on the grid. The minimal cost path from the point where oxygen exits the protein to its origin can be easily found using this information by starting from the exit point and moving toward smaller values in the map of arrival times (going down the gradient). This was implemented by integrating the steepest descent using the standard 4th order Runge-Kutta method. Solution of this equation requires calculation of the gradient at any point inside the three dimensional map of the first arrival time. The gradients were calculated using the intermediate differences approach [5], which introduces less smoothing than the conventional central differences method and in our case produced clearer results. To calculate the potentials of mean force (PMF) the free energy map was projected onto the minimal energy paths.

2.4. Umbrella sampling simulations

Unbiased molecular dynamics simulations produce an ensemble of conformational states from which free energy profiles representative of a dynamic protein can be calculated by averaging the free energies determined from many individual conformational "snapshots". In PSII potential energy barriers in water and oxygen channels leave some areas relatively poorly populated by explicit ligands (water or O_2) and thus poorly sampled or completely unsampled in unbiased simulations. Umbrella sampling [34] is a means of sampling these energetically unfavorable and thus relatively inaccessible states in molecular dynamics simulations. This is achieved by using a suitable energetic bias to increase the sampling of relevant higher energy states. Once the biased simulations are finished, the effect of the energetic bias on the simulations is reverted to allow evaluation of the properties of the unbiased system.

All channels were divided into 0.5 Å-wide equidistant sections parallel to the channel direction, with the center of each section representing an umbrella center. Subsequently, oxygen or water ligands were placed into the channel at the umbrella center. In the case of oxygen umbrella sampling the water molecule that physically overlapped the placed oxygen was removed. In the case of water umbrella sampling the biasing potential was applied to the water molecule nearest to the umbrella center. Umbrella sampling calculations were carried out by applying a harmonic restraint force along the pore coordinate with force constants between 10 and 40 kcal/mol·Å^2. In water, the oxygen atom was restrained; in O_2, a dummy atom centered between the two oxygen atoms was restrained. Additionally, the explicit water or O_2 molecule was restrained to a cylinder of radius 3 Å whose axis was centered along the pore by applying an additional harmonic force $F(r) = -kc(r - rc)\,\mathrm{H}(r - rc)$ pointing toward the cylinder axis. Here r denotes the distance from the cylinder axis, $kc = 100$ the force constant in kcal/mol·Å^2, and H is the Heaviside step function.

2.5. Calculation of PMFs

All five water channels, described in our previous work [38] and 3 additional channels found in the present study using ILS simulations were subjected to the umbrella sampling simulations. A series of simulations with different biases designed to restrain a solute at multiple positions along each of the channels were performed. Distributions of the positions of the restrained atom along all channels were extracted from the positions of the restrained atom. It was ensured that these histograms overlapped well along the entire channel i.e. all positions along the channel were well sampled, so that the lowest density location was sampled not less than half as often as the highest density location. In the case of poor sampling density near the maxima in the PMF, additional umbrella simulations with higher force constants were performed.

One complete umbrella sampling for each of the channels included 50–90 independent simulations with oxygen or water probe molecules inserted at different positions along the channel (the number of positions dependent upon the channel length) carried out for 200 ps. The starting frames for the umbrella sampling simulations at different probe positions were taken randomly from a 10-ns equilibrium simulation of PSII. Before collecting the histograms the system was equilibrated for 200 ps to allow it to relax after insertion of the probe molecule. Complete umbrella sampling for each channel was repeated five times. In total, 3860 histograms were collected from 772 ns of simulation.

Histograms obtained with the different biases were combined using the weighted histogram formalism as implemented in the WHAM program [15] to allow for the computation of unbiased free energy profiles along the channels. Statistical errors were calculated using bootstrap analysis as described in [19]. Complete PMFs of each channel were constructed N times by randomly selecting histograms from all 5 available simulations. Bootstrapping was done 100

times, yielding 100 PMFs for each channel from which the average and standard deviations were calculated.

3. Results

3.1. Three major routes for oxygen diffusion within PSII as revealed by ILS simulations

To identify the diffusion pathways we calculated a 3D free energy map for oxygen within PSII using ILS as previously described [43], see Fig. 2A. The 3D free energy map reveals areas within the protein where oxygen has a high probability of residing. We found a complex free energy landscape with a large number of oxygen binding cavities. Two areas near the catalytic site of PSII with high binding affinities for oxygen are particularly suitable for the initial localization of oxygen, these are shown as *s1* and *s2* in Fig. 2A and C. Oxygen binding site *s1* is in direct contact with water molecule w_2^* near the so called "dangling" Mn(4) which has previously been suggested to be a binding site for one of the two substrate water molecules of the water splitting reaction [32]. Site *s2* is separated from both putative substrate water binding sites w_1^* and w_2^* by D1-V185 and D1-E189. Sites *s1* and *s2* are separated from each other by water molecule w_2^* and D1-V185. After completion of the water oxidation reaction, w_2^* would be converted into protons and molecular oxygen and thus both sites could be accessible to the oxygen product.

The complex nature of the potential energy map made it impossible to directly observe distinct oxygen pathways leading from the OEC to the bulk solvent. To identify the most likely routes for oxygen diffusion from the active site to the protein surface we searched for low-energy paths within the 3D energy maps, as previously described [43], by solving the Eikonal equation for wave front propagation through heterogeneous media (where the "slowness" of the media is proportional to the energetic cost function) using the finite-differences method. This allowed us to construct pathways through the free-energy landscape that could be considered the fastest and most energetically preferred routes of oxygen diffusion.

In our original application of this technique, we described only the lowest energy path which originated at the s1 site and split into two exit points. In this work we have extended our analyses to follow the propagation of waves originating from both the *s1* and *s2* sites which revealed two distinct channel systems leading to the bulk solvent (Fig. 2B) from either side of the OEC. The wave initiated in one of the two proximal binding sites did not overlap with the wave initiated at the other site indicating the presence of an energetic barrier between these two sites. As previously described [43], the lowest energy pathway originated at the *s1* site and split in two branches exiting from the protein at two distant sites (*e1* and *e2*). The wave originating at the *s2* site revealed a slightly higher energy pathway, Fig. S2, which exited the protein at *e3*. By back-tracing the propagation of the wave fronts from these exit points to the source of the waves we identified three major channels with a high probability of oxygen occupancy connecting the protein surface with the active site (Fig. 2C).

3.2. Oxygen channels in PSII are closely related to water channels

The free energy map indicated that the hydrophobic transmembrane regions of PSII did not exhibit a higher probability for oxygen occupancy than the extrinsic parts of the protein complex. All three oxygen channels, as revealed by ILS simulations, are located within the hydrophilic part of PSII protruding into the thylakoid lumen. In addition to the full channels connecting active site with the bulk solvent we observed the wavefront propagating into the hydrophobic

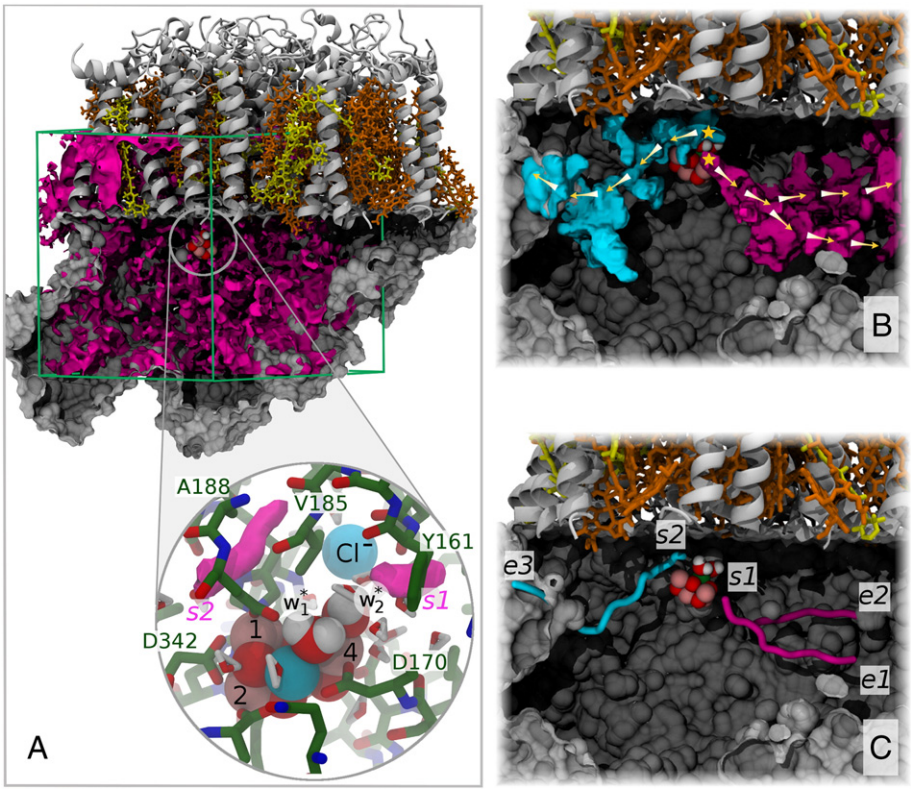

Fig. 2. Steps in the discovery of oxygen channels. (A) Free energy map of oxygen (shown in purple) obtained using ILS and overlapped with PSII. The enlarged zoom-in area shows the neighborhood of OEC. Two proposed substrate water molecules and chloride ion are shown as spheres. Two areas with high oxygen binding affinity (*s1* and *s2*) are shown as pink surfaces. (B) Snapshot of wave front propagations through the free energy map of PSII showing the fastest pathways of oxygen diffusion away from *s1* (purple isosurface) and *s2* (cyan isosurface). The locations of the wave sources are marked by yellow stars. (C) The minimal energy paths obtained by backtracing the wave fronts from their exit points to their respective starting points.

transmembrane region of the reaction center. This wavefront terminated near the photochemically active reaction center chlorophyll dimer P680 as shown in Fig. 3. Thus results of this study confirmed our initial observation that oxygen cannot easily diffuse into the hydrophobic transmembrane area of PSII [43].

An animation of the wave front propagation through the free energy map of PSII overlapped with the molecular dynamics trajectory is available online as Video S1. This animation demonstrates the correlation between the dynamics of oxygen and internal water molecules within the PSII protein.

As described previously [43] the two oxygen channels arising from the *s1* site (*s1-e1* and *s1-e2*, see Fig. 2C) showed significant overlap with water channel 4 as defined in [38] The new oxygen channel we found originating at the *s2* site (*s2-e3*, see Fig. 2C) has significant overlap with water channel 1 as defined in [38]. For consistency with previous work with water channels we denoted the oxygen channels identified by the ILS technique as channel 1i, channel 4ai and channel 4ci, as shown in Fig. 4. Fig. 4 also shows the five previously described water channels from [38]. All three oxygen channels identified above and five channels that were previously identified as water channels in [38] were selected for accurate determinations of the potential of mean force (PMF), for both explicit water and explicit oxygen molecules, using umbrella sampling simulations.

3.3. Several channels in PSII are highly permeable for oxygen

The potentials of mean force for the permeation of oxygen through all identified channels are summarized in Fig. 5. As seen from this figure the channels exhibit a wide variety of energy profiles with very different energetic barriers as oxygen moves from the OEC towards bulk water in the lumen.

Channels 4a, 4ai, 4ci, 1, and 1i are characterized by having relatively low permeation barriers in the range of 2.8–6.9 kcal/mol while channels 4b, 2 and 3 have much higher permeation barriers >12 kcal/mol. Channel 4a and its ILS analog, channel 4ai, have the lowest permeation barriers of all channels. The main permeation barrier of channel 4ai is higher than the main barrier of channel 4a by only 2.2 kcal/mol. This barrier is located near the origin of the channel and arises from the increase in free energy required for the oxygen to escape from the high affinity area *s1*. As channel 4a begins near the substrate water binding site w_1*, outside of the *s1* area, it does not have to cross this first barrier. Channels 4a and 4ai merge at a distance about 8 Å from the OEC and follow very similar paths afterwards. The permeation barriers over the rest of channel 4ai are higher than in channel 4a by only 1 kcal/mol.

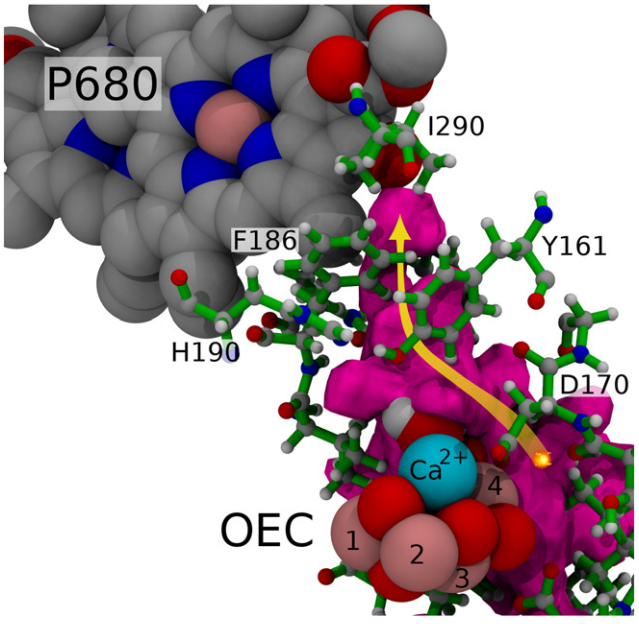

Fig. 3. Snapshot of the wave front propagation in the free energy map of PSII showing oxygen diffusion from the catalytic site towards the reaction center pigment P680 (purple isosurface).

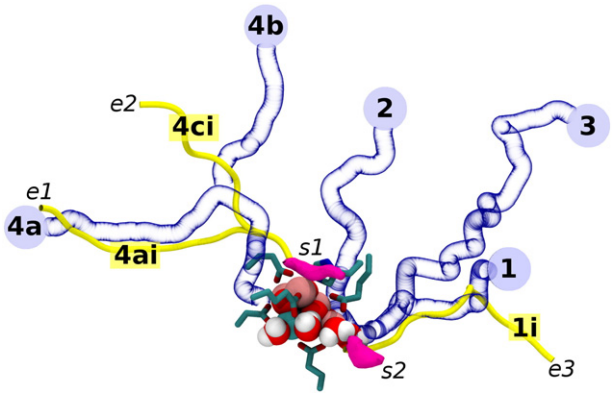

Fig. 4. Topology of the channel system in PSII. Blue tubes represent previously found water channels, and yellow tubes represent oxygen channels found using the ILS method. Two areas near the OEC with high oxygen binding affinity (*s1* and *s2*) are shown as purple surfaces. Orientation is shown as in Fig. 1 of ref. [13].

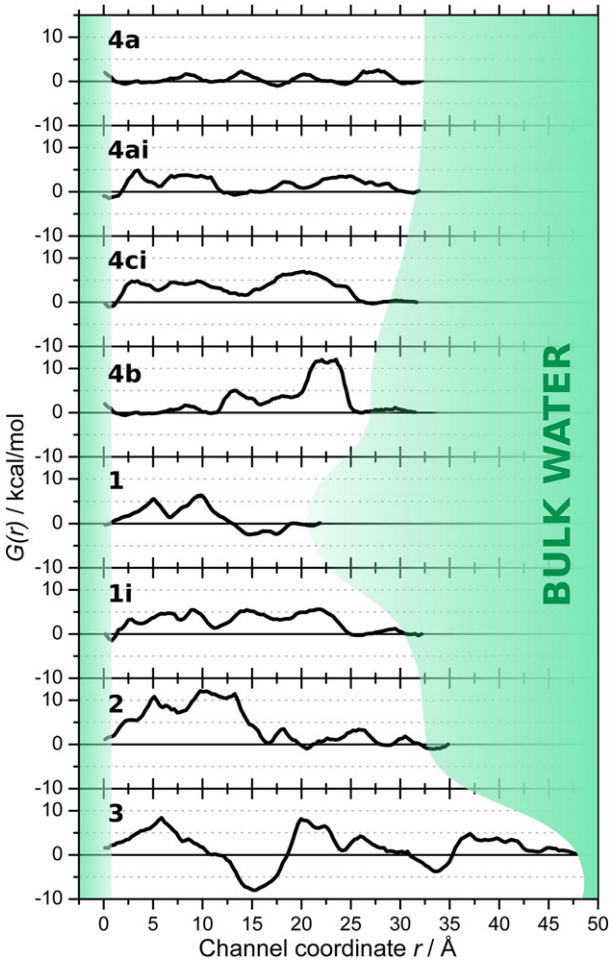

Fig. 5. Potentials of the mean force $G(r)$ of all identified channels for oxygen obtained using umbrella sampling simulations. Potentials are relative to that calculated for oxygen in the bulk aqueous solution which was set to zero. See text and Fig. 4 for details of channel identification. Values are means calculated from bootstrap analysis of five independent simulations, see Methods section for details. Standard deviations were usually within 10%, see Table 1 for representative values.

If we assume the permeability to be proportional to $\exp(-\Delta G_{max}/k_BT)$, where ΔG_{max} is the maximum barrier height, k_B is the Boltzmann constant, and T is the temperature, we can estimate the relative differences in permeability between the channels. Thus, the initial 2.2 kcal/mol higher barrier in channel 4ai corresponds to a reduction of permeability by a factor of 40 at this point and the second 1 kcal/mol difference would reduce the permeability of channel 4ai by 5 times in this region.

3.4. Selectivity mechanism of O_2 permeation in PSII

A comparison of the oxygen free energy profiles shown in Fig. 5 with the previously determined free energy profiles for water permeating through the same channels [38] often revealed striking differences in the permeation of these two solutes. For example, a 10 kcal/mol barrier for water previously observed in the common part of channels 4a/4b [38] was only 1.7 kcal/mol in the free energy profile of oxygen, while a 6 kcal/mol barrier to water in the distal part of channel 4b was 12 kcal/mol for oxygen. However, as the previous study of water permeation was done using a different method (MSMD), and using implicit bulk water, we repeated the determination of water free energy profiles through all channels using the same simulation protocol as was used for oxygen. This allowed a direct comparison of energetic barriers for oxygen and water which are summarized in Table 1.

The data in Table 1 and supplementary Fig. S1 show pronounced differences between permeation barriers for water and oxygen. While most barriers are higher for water than for oxygen, some barriers exhibit the opposite dependence on solute. Good examples of both types of differential permeability are found in the channel 4 system, and full free energy profiles for both solutes are shown in Fig. 6. Two major barriers are observed in channel 4b as it leads from the OEC to the lumen. The closest barrier to the OEC, "*B1*", is only a barrier for water whereas the "*B2*" region, close to the lumen, is much less permeable for oxygen than it is for water.

A closer look at the structure and dynamics of water at these constriction sites revealed that *B1* is characterized by a hydrophobic ridge (formed by D2-L352 and CP43-V410) between two hydrophilic cavities filled with water. On both sides of *B1* water molecules are stabilized by favorable interactions with the protein residues D1-D342 and E329 and other water molecules (Fig. 6B). Passage of water through *B1* is impaired by a reduction of these favorable interactions and the relatively small size of the pore, which is only able to accommodate one water molecule. In contrast, hydrophobic oxygen, having no favorable interactions outside of the *B1* site does not require activation energy to pass through this area. Interestingly, D2-L352, D1-D342 and D1-E329 are conserved across all cyanobacterial PSII sequenced to date, and CP43 has either Val or Ile at position 410. In contrast to *B1*, *B2* is more permeable for water than for oxygen. As shown in Fig. 6C, a water molecule in the center of the B2 region is stabilized by the formation of three hydrogen bonds, one with the carboxyl terminal of PsbU and two with the polar backbone atoms of PsbV G132 and V135, respectively. However, upon passage of oxygen through *B2* these favorable interactions between water and protein are disrupted and the free energy increase is not compensated for by weak interactions of the apolar oxygen with the protein.

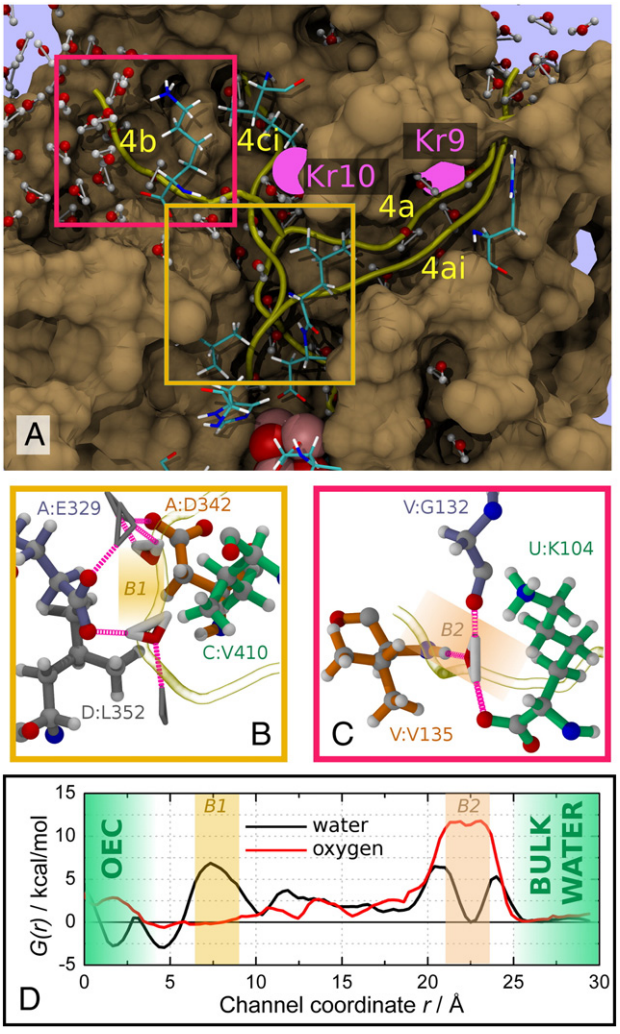

Fig. 6. (A) Snapshot of an MD simulation showing the region containing channels 4a, 4ai, 4b and 4ci. Water molecules inside the channels are represented in ball and stick. The locations of two Kr binding sites from [13] are shown as purple spheres. Channels originate at the OEC, bottom center, and are shown as yellow color tubes. (B), (C) Selected protein residues involved in the formation of barriers B1 and B2, respectively, within channel 4b. (D) Free energy profiles for water and oxygen permeating through channel 4b. Free energies are relative to that of either water or oxygen, respectively, in the bulk aqueous solution which was set to zero for both.

The key finding here is that the *B1* site, buried deep within the PSII protein, serves as a selectivity filter, restricting the access of water and other polar solutes to the OEC while allowing completely unrestricted passage of oxygen. The energetic barrier for water also exceeds the energetic barrier for oxygen within channels that originate from the other side of the OEC, near the s2 site, However a different mechanism is responsible in channel 1 where the major factor defining the difference in permeability is the small size of the pore

Table 1
Summary of the main free energy barriers ΔG_{max} for permeation of oxygen and water in kcal/mol.

	4a	4ai	1	1i	4ci	4b	2	3
O_2	–	4.9 ± 0.4	5.8 ± 1.2	5.4 ± 0.9	4.8 ± 0.4	–	10.8 ± 1.2	8.4 ± 0.6
	2.2 ± 0.5	3.8 ± 0.7	6.3 ± 0.5	5.5 ± 1.5	6.9 ± 0.7	11.8 ± 0.4	12.1 ± 1.1	16.1 ± 1.8
	2.6 ± 0.6	–	–	–	–	–	–	8.5 ± 1.3
H_2O	6.8 ± 0.6	8.7 ± 2.0	3.8 ± 1	11.1 ± 0.5	6.3 ± 0.9	6.9 ± 0.6	10.8 ± 2.1	7.5 ± 1.9
	4.6 ± 0.9	8.0 ± 1.9	10.1 ± 1	10.7 ± 1.0	7.3 ± 1.1	6.5 ± 0.7	8.3 ± 1.3	12.8 ± 1.9
	–	–	–	–	–	–	8.8 ± 0.5	7.7 ± 0.8

Permeation barriers are listed in their relative order of distance from the OEC. The potentials of mean force for the permeation of water through all identified channels are available in Supplementary Fig. S1. Fig. S1 also identifies the location of each permeation barrier.

which makes it easier for oxygen with its smaller VDW radius to traverse it.

4. Discussion

4.1. Oxygen channel topology

All oxygen exit pathways showed large regions of overlap with water channels previously discovered in MD studies [37,38] and with water and proton channels previously described in cavity analyses of static structures [13,18,25]. It was interesting that none of the oxygen pathways led apolar molecular oxygen to the hydrophobic intermembrane region. Our results indicate that within PSII oxygen moves through water channels rather than selective hydrophobic oxygen channels and is delivered to bulk water in the lumen and not to the thylakoid membrane.

Using explicit ligand approaches we characterized the relative permeability of oxygen and water through the pathways identified in this study as well as previously described channels. Fig. 7 summarizes our results and emphasizes our finding that all channels permeable to oxygen were also permeable to water. It is also clear from Fig. 7 that the previous description of two distinct complex channel systems for water, one approaching the OEC from the Ca^{2+} side and the other from the dangling Mn side [37,38] is also observed for oxygen. The three branches of channel 4 originating from the Ca^{2+} side of the OEC have the lowest energy barriers for oxygen and overlap the area that had first been identified in static structures as the “large” channel system [18]. This large channel system had previously been suggested to carry oxygen as well as water.

Our computational characterization of oxygen channel topology is in good agreement with high pressure Krypton crystallography as the two Kr binding sites found in that study [13] are located along the two channels we determined to have the lowest barriers to oxygen permeation, 4a and 4ci (Fig. 6). Channels 1 and 1i on the dangling Mn side of the OEC exhibit only slightly higher energetic barriers to oxygen. Oxygen is thus released from PSII via several highly permeable channels, which also carry water. The release of oxygen from the protein is essentially unconstrained.

4.2. Controlled/restricted access of water vs. fast unrestricted oxygen exit

Early hypotheses concerning oxygen and water pathways through PSII were based on the ideas that water supply may be restricted or controlled to protect the OEC, and that oxygen exhaust should be unrestricted to prevent unwanted oxidative damage. The differing physical characteristics of the small apolar oxygen molecule and the larger polar water molecule supported the idea that the different requirements for water and oxygen transport would likely be served by channels specific for each solute. Our results are consistent with different permeabilities of oxygen and water, but as summarized in Fig. 7, we found no channels that were specific for only molecular oxygen. However, comparison of the free energy profiles for the permeation of oxygen to those for the permeation of water revealed in all cases that access of water to the catalytic site required significantly higher activation energy than did the release of oxygen. While the lowest permeation barrier for water was 6.8 kcal/mol the lowest barrier for oxygen was only 2.6 kcal/mol. This corresponds to a 1100 times higher permeation rate of oxygen as compared to water.

Thus, within the same channel systems, regulatory mechanisms control water flow and access to the Mn_4CaO_5 cluster, but allow oxygen to leave PSII with minimal restriction. We found that combinations of small pore size and/or hydrophobic ridges bracketed by larger hydrophilic regions were responsible for the selective barriers to water over oxygen.

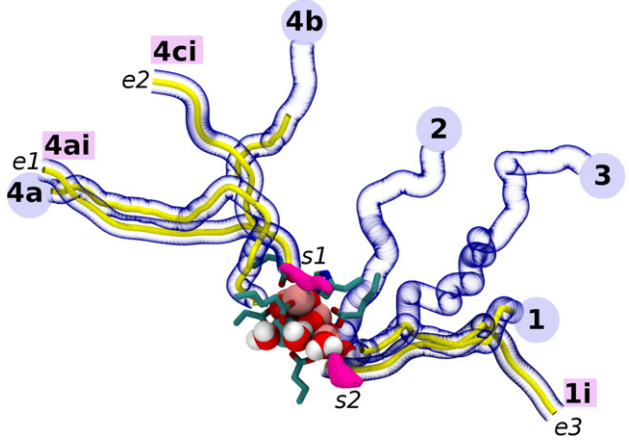

Fig. 7. Topology of the channel system in PSII. Blue tubes represent channels which are permeable for water, and yellow tubes represent channels highly permeable for oxygen. Two areas near the OEC with high oxygen binding affinity (*s1* and *s2*) are shown as purple surfaces.

4.3. Oxygen channels in other enzymes

Cytochrome c oxidase is an integral membrane protein complex that shares a number of features with PSII. It has an active site buried within the protein and requirements for the transport of water, protons and oxygen. However, unlike PSII, cytochrome c oxidase reduces its molecular oxygen substrate, takes up protons and releases water as product. Oxygen is supplied to the active site via a diffusion channel that has been well characterized by extensive Xe gas pressurization crystallography [24] and does not contain water. The oxygen channel is a large hydrophobic Y-shaped channel that connects the $a_3 - Cu_B$ center in the active site of the complex to two hydrophobic regions on the surface of the protein buried within the lipid bilayer. Clusters of water molecules occupying a cleft between subunit I and subunit II of the complex are believed to be involved in proton transport to, and water removal from, the active site.

Although PSII and cytochrome c oxidase both require efficient transport of oxygen, the former benefits by minimizing the concentration and the latter by maximizing the concentration at the active site. This functional difference translates into very different structural organizations. In cytochrome c oxidase a selective hydrophobic channel connecting the active site of cytochrome c oxidase with the oxygen rich membrane ensures maximal substrate density. In PSII the oxygen release channels avoid contact with the membrane and direct oxygen towards multiple aqueous exit sites characterized by much lower effective oxygen concentrations than the membrane. This organization maximizes the removal of oxygen from the active site and minimizes its potentially dangerous contact with PSII chromophores.

In both PSII and cytochrome ba_3 oxidase significant rearrangements within the protein are not necessary for oxygen permeation likely because both systems benefit from fast permeation for activity. In contrast, gas diffusion in heme nitric oxide/oxygen binding (H-NOX) domains from the family of gas-sensing proteins does not occur through discrete, continuous channels. In these systems, protein dynamics controls O_2 and NO diffusion through transiently formed pathways [41]. This restricted diffusion would facilitate the trapping of O_2 at the heme iron [45], a strategy which may be important for anaerobic organisms to sense low amounts of O_2.

4.4. Channel free energy profiles in design of mutations to block the channel network

Our umbrella sampling simulation is the first investigation of the energetic cost of moving oxygen through putative channels within PSII. However, until more is known concerning the structural changes of the OEC associated with progression of the S-states and formation

of molecular oxygen the details of oxygen delivery from the active site to the two major channel systems will remain obscure to computational studies. It is thus not clear how many of the possible pathways are functionally relevant. Results of our study do, however, open the possibility of testing the potential roles of individual water/oxygen channels in modulating substrate/product migration by designing mutations targeting regions in each branch of the tunnel network at sites relatively distant from the OEC.

Supplementary data to this article can be found online at http://dx.doi.org/10.1016/j.bbabio.2013.06.008.

Acknowledgement

This work was supported by Discovery and Equipment grants from the Natural Science and Engineering Research Council of Canada. It was made possible by the facilities of the Shared Hierarchical Academic Research Computing Network (SHARCNET) and Compute/Calcul Canada and partial support from DOE #DE-SC0001423 “Studies of Photosynthetic Reaction Centers and Biomimetic systems”.

References

[1] J.M. Anderson, Does functional photosystem II complex have an oxygen channel? FEBS Lett. 488 (2001) 1–4.
[2] J. Barber, Photosystem II: the engine of life, Q. Rev. Biophys. 36 (2003) 71–89.
[3] R. Baron, C. Riley, P. Chenprakhon, K. Thotsaporn, R.T. Winter, A. Alfieri, F. Forneris, W.J.H. van Berkel, P. Chaiyen, M.W. Fraaije, A. Mattevi, J.A. McCammon, Multiple pathways guide oxygen diffusion into flavoenzyme active sites, Proc. Natl. Acad. Sci. U. S. A. 106 (2009) 10603–10608.
[4] M. Basma, S. Sundara, D. Calgan, T. Vernali, R.J. Woods, Solvated ensemble averaging in the calculation of partial atomic charges, J. Comput. Chem. 22 (2001) 1125–1137.
[5] M. Bosma, J. Smit, J. Terwisscha, J. van Scheltinga, Super resolution volume rendering hardware, Tenth Workshop on Graphics Hardware, 1995.
[6] D.B. Calhoun, J.M. Vanderkooi, G.V. Woodrow, S.W. Englander, Penetration of dioxygen into proteins studied by quenching of phosphorescence and fluorescence, Biochemistry 22 (1983) 1526–1532.
[7] P.P. Chapagain, C.K. Regmi, W. Castillo, Fluorescent protein barrel fluctuations and oxygen diffusion pathways in mCherry, J. Chem. Phys. 135 (2011).
[8] J. Cohen, A. Arkhipov, R. Braun, K. Schulten, Imaging the migration pathways for O-2, CO, NO, and Xe inside myoglobin, Biophys. J. 91 (2006) 1844–1857.
[9] J. Cohen, K. Kim, P. King, M. Seibert, K. Schulten, Finding gas diffusion pathways in proteins: application to O-2 and H-2 transport in Cpl [FeFe]-hydrogenase and the role of packing defects, Structure 13 (2005) 1321–1329.
[10] R.O. Dror, R.M. Dirks, J.P. Grossman, H.F. Xu, D.E. Shaw, Biomolecular simulation: a computational microscope for molecular biology, Annu. Rev. Biophys. 41 (2012) 429–452.
[11] W. Erker, R. Hubler, H. Decker, Tryptophan quenching as linear sensor for oxygen binding of arthropod hemocyanins, Biochim. Biophys. Acta, Gen. Subj. 1780 (2008) 1143–1147.
[12] K.N. Ferreira, T.M. Iverson, K. Maghlaoui, J. Barber, S. Iwata, Architecture of the photosynthetic oxygen-evolving center, Science 303 (2004) 1831–1838.
[13] A. Gabdulkhakov, A. Guskov, M. Broser, J. Kern, F. Muh, W. Saenger, A. Zouni, Probing the accessibility of the Mn4Ca cluster in photosystem II: channels calculation, noble gas derivatization, and cocrystallization with DMSO, Structure 17 (2009) 1223–1234.
[14] Govindjee, Photosystem II: the light-driven water: plastoquinone oxidoreductase, in: Thomas J. Wydrzynski, Kimiyuki Satoh (Eds.), Volume 22, Advances in Photosynthesis and Respiration, Photosynth. Res., 87, Springer, Dordrecht, The Netherlands, 2006, pp. 331–335.
[15] A. Grossfield, WHAM: the Weighted Histogram Analysis Method, Version 2.0.6, http://Membrane.Urmc.Rochester.Edu 2012.
[16] N. Hansen, F.A.B. Agbor, F.J. Keil, New force fields for nitrous oxide and oxygen and their application to phase equilibria simulations, Fluid Phase Equilib. 259 (2007) 180–188.
[17] F.M. Ho, Uncovering channels in photosystem II by computer modelling: current progress, future prospects, and lessons from analogous systems, Photosynth. Res. 98 (2008) 503–522.
[18] F.M. Ho, S. Styring, Access channels and methanol binding site to the CaMn4 cluster in Photosystem II based on solvent accessibility simulations, with implications for substrate water access, Biochim. Biophys. Acta Bioenerg. 1777 (2008) 140–153.
[19] J.S. Hub, B.L. de Groot, Mechanism of selectivity in aquaporins and aquaglyceroporins, Proc. Natl. Acad. Sci. U. S. A. 105 (2008) 1198–1203.
[20] W. Humphrey, A. Dalke, K. Schulten, VMD—visual molecular dynamics, J. Mol. Graphics 14 (1996) 33–38.
[21] B.J. Johnson, J. Cohen, R.W. Welford, A.R. Pearson, K. Schulten, J.P. Klinman, C.M. Wilmot, Exploring molecular oxygen pathways in Hansenula polymorpha copper-containing amine oxidase, J. Biol. Chem. 282 (2007) 17767–17776.
[22] L. Kale, R. Skeel, M. Bhandarkar, R. Brunner, A. Gursoy, N. Krawetz, J. Phillips, A. Shinozaki, K. Varadarajan, K. Schulten, NAMD2: greater scalability for parallel molecular dynamics, J. Comput. Phys. 151 (1999) 283–312.
[23] J. Kern, B. Loll, A. Zouni, W. Saenger, K.D. Irrgang, J. Biesiadka, Cyanobacterial photosystem II at 3.2 angstrom resolution—the plastoquinone binding pockets, Photosynth. Res. 84 (2005) 153–159.
[24] V.M. Luna, J.A. Fee, A.A. Deniz, C.D. Stout, Mobility of Xe atoms within the oxygen diffusion channel of cytochrome ba(3) oxidase, Biochemistry 51 (2012) 4669–4676.
[25] J.W. Murray, J. Barber, Structural characteristics of channels and pathways in photosystem II including the identification of an oxygen channel, J. Struct. Biol. 159 (2007) 228–237.
[26] P. Podvin, I. Lecomte, Finite-difference computation of traveltimes in very contrasted velocity models—a massively parallel approach and its associated tools, Geophys. J. Int. 105 (1991) 271–284.
[27] A. Roy, P. Carpentier, D. Bourgeois, M. Field, Diffusion pathways of oxygen species in the phototoxic fluorescent protein KillerRed, Photochem. Photobiol. Sci. 9 (2010) 1342–1350.
[28] J. Saam, I. Ivanov, M. Walther, H.G. Holzhutter, H. Kuhn, Molecular dioxygen enters the active site of 12/15-lipoxygenase via dynamic oxygen access channels, Proc. Natl. Acad. Sci. U. S. A. 104 (2007) 13319–13324.
[29] J. Saam, E. Rosini, G. Molla, K. Schulten, L. Pollegioni, S. Ghisla, O-2 reactivity of flavoproteins dynamic access of dioxygen to the active site and role of a H+ relay system in D-amino acid oxidase, J. Biol. Chem. 285 (2010) 24439–24446.
[30] C. Simmerling, B. Strockbine, A.E. Roitberg, All-atom structure prediction and folding simulations of a stable protein, J. Am. Chem. Soc. 124 (2002) 11258–11259.
[31] Y.F. Song, J.J. Mao, M.R. Gunner, MCCE2: improving protein pK(a) calculations with extensive side chain rotamer sampling, J. Comput. Chem. 30 (2009) 2231–2247.
[32] E.M. Sproviero, J.P. McEvoy, J.A. Gascon, G.W. Brudvig, V.S. Batista, Computational insights into the O-2-evolving complex of photosystem II, Photosynth. Res. 97 (2008) 91–114.
[33] R.F. Tilton, I.D. Kuntz, G.A. Petsko, Cavities in proteins—structure of a metmyoglobin-xenon complex solved to 1.9-A, Biochemistry 23 (1984) 2849–2857.
[34] G.M. Torrie, J.P. Valleau, Non-physical sampling distributions in Monte-Carlo free-energy estimation—umbrella sampling, J. Comput. Phys. 23 (1977) 187–199.
[35] Y. Umena, K. Kawakami, J.R. Shen, N. Kamiya, Crystal structure of oxygen-evolving photosystem II at a resolution of 1.9 angstrom, Nature 473 (2011) 55–60.
[36] S. Vasil'ev, D. Bruce, A protein dynamics study of photosystem II: the effects of protein conformation on reaction center function, Biophys. J. 90 (2006) 3062–3073.
[37] S. Vassiliev, P. Comte, A. Mahboob, D. Bruce, Tracking the flow of water through photosystem II using molecular dynamics and streamline tracing, Biochemistry 49 (2010) 1873–1881.
[38] S. Vassiliev, T. Zaraiskaya, D. Bruce, Exploring the energetics of water permeation in photosystem II by multiple steered molecular dynamics simulations, Biochim. Biophys. Acta Bioenerg. 1817 (2013) 1671–1678.
[39] J.M. Wang, P. Cieplak, P.A. Kollman, How well does a restrained electrostatic potential (RESP) model perform in calculating conformational energies of organic and biological molecules? J. Comput. Chem. 21 (2000) 1049–1074.
[40] Y. Wang, J. Cohen, W.F. Boron, K. Schulten, E. Tajkhorshid, Exploring gas permeability of cellular membranes and membrane channels with molecular dynamics, J. Struct. Biol. 157 (2007) 534–544.
[41] M.B. Winter, M.A. Herzik, J. Kuriyan, M.A. Marletta, Tunnels modulate ligand flux in a heme nitric oxide/oxygen binding (H-NOX) domain, Proc. Natl. Acad. Sci. U. S. A. 108 (2011) E881–E889.
[42] T. Wydrzynski, W. Hillier, J. Messinger, On the functional significance of substrate accessibility in the photosynthetic water oxidation mechanism, Physiol. Plant. 96 (1996) 342–350.
[43] T. Zaraiskaya, S. Vassiliev, D. Bruce, Revealing molecular oxygen migration pathways in photosystem II using implicit ligand sampling and wavefront propagation, J. Comput. Sci. 4 (2013), (in press).
[44] L. Zhang, J. Hermans, Hydrophilicity of cavities in proteins, Proteins Struct. Funct. Genet. 24 (1996) 433–438.
[45] Y.B. Zhang, M. Lu, Y.K. Cheng, Z.Q. Li, H-NOX domains display different tunnel systems for ligand migration, J. Mol. Graph. Model. 28 (2010) 814–819.